EPJ Web of Conferences **70**, 00023 (2014)
DOI: 10.1051/epjconf/ 20147000023

Overview of results from ALICE at the CERN LHC

Panos Christakoglou[1,a] (for the ALICE Collaboration)

[1] *Nikhef, Science Park 105, 1098 XG Amsterdam, The Netherlands*

Abstract. ALICE (A Large Ion Collider Experiment) at the Large Hadron Collider (LHC) has been running successfully for more than two years, recording both pp and Pb–Pb data. The analysis of these data samples revealed intriguing properties of the produced matter. They indicate that the system created in heavy–ion collisions, is larger, hotter and denser compared to the one created at lower energies. In this article, I review the latest experimental results from ALICE from both the 2010 and the 2011 run.

1 Introduction

As the early universe evolved, a transition occurred at temperatures T = 150–200 MeV, related to the spontaneous breaking of chiral symmetry in Quantum Chromo–Dynamics (QCD). The nature of this transition affects our understanding of the evolution of the universe. High–energy heavy–ion collisions provide the opportunity to recreate similar conditions of energy density and temperature in the laboratory, thus allowing the study of the properties of nuclear matter under these extreme conditions. According to lattice (QCD) calculations, at sufficiently high energy densities, with the latest estimates being close to 0.5 GeV/fm^3 [1], normal nuclear matter undergoes a transition to a state where the constituents, the quarks and the gluons, are deconfined [2]. This state of matter is called the Quark–Gluon–Plasma (QGP). Convincing experimental evidences of the existence of a deconfined phase have been published already at RHIC energies [3]. Recently, the first experimental results from the LHC heavy–ion program [4, 5] provided additional evidence related to the existence of this new state of matter at this new energy regime. Hence, the focus now turns towards the study of the properties of the QGP. In this article, I review the latest experimental results from the analysis of Pb–Pb collisions at $\sqrt{s_{NN}}$ = 2.76 TeV, recorded with the ALICE detector at the LHC [6, 7].

2 Bulk properties

One of the first measurements performed at the LHC was related to the number of particles produced per unit of pseudo–rapidity ($dN_{ch}/d\eta$). The charged particle multiplicity was measured in the central rapidity region ($|\eta| < 0.5$) using tracklets measured by the Inner Tracking System (ITS) and tracks reconstructed by the Time Projection Chamber (TPC). In [8], it was reported that $dN_{ch}/d\eta \approx 1600$, for the 5% most central Pb–Pb collisions. This value compared to the $dN_{ch}/d\eta \approx 690$ reported by RHIC experiments for the 5% most central Au–Au collisions [9], marks an increase of ≈ 2.3. The

[a] e-mail: Panos.Christakoglou@nikhef.nl

measured $dN_{ch}/d\eta$ can be used to extract an estimate of the energy density using the formula discussed by Bjorken in [10]. The value reported at the LHC could be translated to an initial energy density of about $\epsilon = 15$ GeV/fm^3 [11] which is almost three times higher than the corresponding value reported at RHIC [3].

2.1 Particle spectra

The system produced after a heavy–ion collision undergoes an expansion during which it demonstrates collective behaviour and can be described in terms of hydrodynamics [12]. The yields and the transverse momentum spectra of identified particles are probing the collective and thermal properties of this produced matter. In particular, the $p_{\rm T}$ distributions reflect the kinetic freeze–out temperature ($T_{kin.}$) and the collective radial flow quantified by the average transverse velocity $\langle\beta_T\rangle$.

Figure 1 presents the $p_{\rm T}$ spectra of pions, kaons and protons as measured by ALICE for the 5% most central Pb–Pb collisions [13]. Positive and negative particles were combined in this plot since they were found to be compatible within the statistical uncertainties. The measurement has been performed in the transverse momentum range from 0.1 up to 4.5 GeV/c at mid–rapidity ($|y| < 0.5$), combining information from the ITS, the TPC and the Time Of Flight (TOF). The feed–down corrected spectra measured at the LHC are compared to results from Au–Au collisions at $\sqrt{s_{NN}} = 200$ GeV, reported by STAR [14] and PHENIX [15]. At the LHC the spectra are harder, indicative of a system exhibiting larger radial flow compared to the RHIC energies. Also shown in Fig. 1 are curves extracted from hydrodynamical calculations [16–18]. All models yield a good agreement with the data points, with the exception of VISH2+1 that misses both the shape and the abundance of protons, probably due to the lack of implementation of the hadronic phase. Finally, the data are fitted with a blast wave parameterization [19], that allows to extract the values of the kinetic freeze–out temperature $T_{kin.} = 96 \pm 10$ MeV and of the collective radial flow velocity $\langle\beta_T\rangle = 0.65 \pm 0.02$. Compared to central Au–Au collisions at RHIC and for a similar $p_{\rm T}$ range, the LHC value for $\langle\beta_T\rangle$ is 10% higher, while $T_{kin.}$ remains similar within errors.

2.2 Elliptic flow

Anisotropic flow is an important observable for probing the properties of the system created in heavy–ion collisions. In non–central collisions, the initial spatial anisotropy of the overlap region of the colliding nuclei is transformed into an anisotropy in momentum space, through interactions between the produced particles. This anisotropy is usually characterised by the Fourier coefficients [20]

$$\mathrm{v}_n = \langle\cos\left[n(\varphi - \Psi_n)\right]\rangle, \tag{1}$$

where φ is the azimuthal angle of the particle, Ψ_n is the azimuthal angle of the initial state spatial plane of symmetry, and n is the order of the flow harmonic. The second Fourier coefficient, v_2, is the elliptic flow and its first measurement at the LHC [4] indicated that the system still behaves as a strongly interacting liquid with a small value of the shear viscosity over entropy ratio η/s. An additional constrain to the value of η/s could be given by studying the elliptic flow in a more differential way i.e. as a function of centrality and transverse momentum for different particle species. Hydrodynamic model calculations predict a characteristic dependence of v_2 on the particle mass at low values of transverse momentum ($p_{\rm T} < 2$ GeV/c). This dependence is induced by the collective radial expansion of the system, which being cumulative throughout the whole collision, has a significant contribution from the partonic phase. However, the hadronic rescattering that follows might mask the information

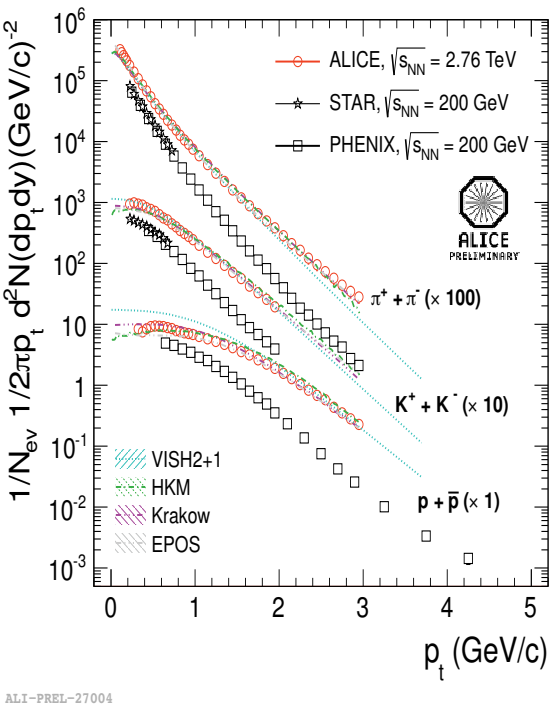

Figure 1. Transverse momentum spectra for pions, kaons and protons (charged combined) measured by ALICE [13], compared to measurements from RHIC [14, 15] and hydrodynamical calculations [16–18].

of the early stage. Hence it is important to use particles that could potentially have small hadronic cross section to probe the early stage of the collision.

Figure 2–left shows the p_{T} differential v_2 for different particle species (i.e. π, K, K^0_s, $\bar{\mathrm{p}}$, Λ, ϕ) measured by ALICE in the 10–20% centrality range. The charged hadrons i.e. π, K and $\bar{\mathrm{p}}$ have been identified using the information from the TPC and the TOF. The neutral particles were measured using their decay products i.e. $K^0_s \rightarrow \pi^+ + \pi^-$, $\Lambda \rightarrow p + \pi^-$ ($\bar{\Lambda} \rightarrow \bar{p} + \pi^+$) and $\phi \rightarrow \mathrm{K}^+ + \mathrm{K}^-$. A clear mass ordering is seen in the low p_{T} region (i.e. $p_{\mathrm{T}} \leq 2$ GeV/c), attributed to collective radial flow that shifts heavy particles to higher values of p_{T}. The experimental points are compared to hydrodynamical calculations [16] using a value of $\eta/s = 0.2$ and the Color Glass Condensate (CGC) initial conditions, represented by the solid curves. It is seen that the model reproduces the p_{T} dependence of v_2 for pions and kaons up to $p_{\mathrm{T}} \approx 2$ GeV/c but overestimates v_2 for heavier particles. However, the inclusion of the hadronic phase improves the agreement with the data points.

At higher values of p_{T}, one of the important experimental findings at RHIC energies was that particles seemed to cluster based on their type i.e. mesons vs baryons [21]. This was interpreted as a sign that hadron formation is dominated by quark coalescence at the end of the partonic evolution. Figure 2–left presents the elliptic flow scaled by the number of constituent quarks, n_q (n_q = 2 and 3 for mesons and baryons, respectively), as a function of the transverse kinetic energy expressed by

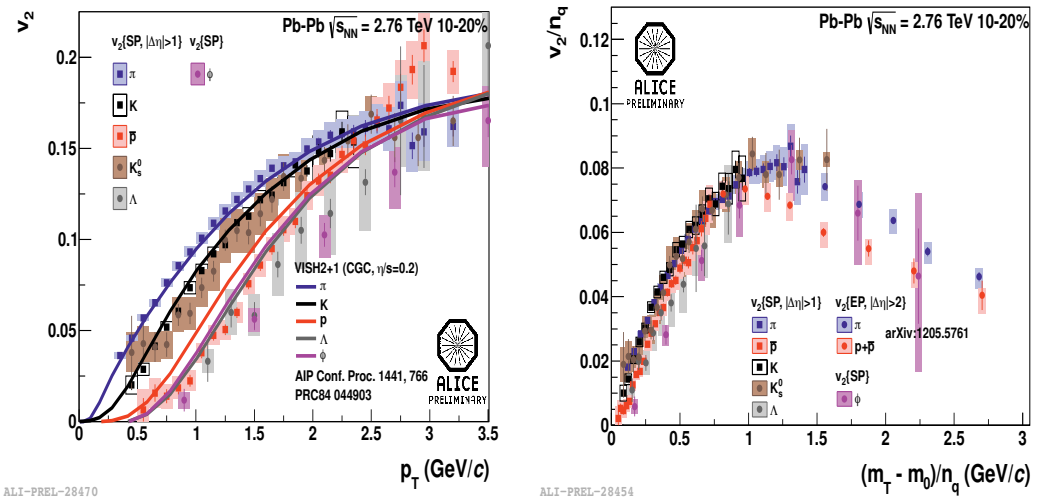

Figure 2. (Left) The p_{T} differential v_2 for different particle species. (Right) The dependence of v_2/n_q on the transverse kinetic energy. In both plots, the 10–20% centrality bin is shown.

$KE_{\mathrm{T}} = (m_{\mathrm{t}} - m_0)$ scaled again by n_q. It is seen that the scaling is broken at the level of 20% throughout the entire p_{T} region.

3 High–p_{T} probes and jets

Particles with large transverse momentum constitute valuable tools to study the hot and dense matter created in a high–energy collision. Such hard probes originate from partonic scatterings with large momentum transfer and thus are directly related to the fundamental QCD degrees of freedom. High p_{T} partons produced in the initial stage of a nucleus–nucleus collision are expected to undergo multiple interactions inside the collision region prior to hadronisation. The energy of the partons is reduced through collisional energy loss and medium–induced gluon radiation. Parton energy loss, not only depends on the density of the created system but also on its ratio of quarks to gluons and on the p_{T} spectra of the scattered partons. The measurement of the energy loss at the LHC will allow to shed some light in the production and propagation of these high–p_{T} probes and to explore the underlying physical mechanisms.

To investigate suppression effects, it is useful to compare single inclusive particle spectra in nuclear collisions to expectations from superposition of independent nucleon–nucleon collisions. This is usually done using the so–called nuclear modification factor R_{AA} defined as the ratio of particle yields in A–A collisions to the pp yield scaled by the number of binary collisions, as in Eq. 2.

$$R_{AA} = \frac{(1/N_{evt.}^{AA}) d^2N_{ch}^{AA}//dp_{\mathrm{T}}d\eta}{\langle N_{coll}\rangle (1/N_{evt.}^{pp}) d^2N_{ch}^{pp}/dp_{\mathrm{T}}d\eta} \tag{2}$$

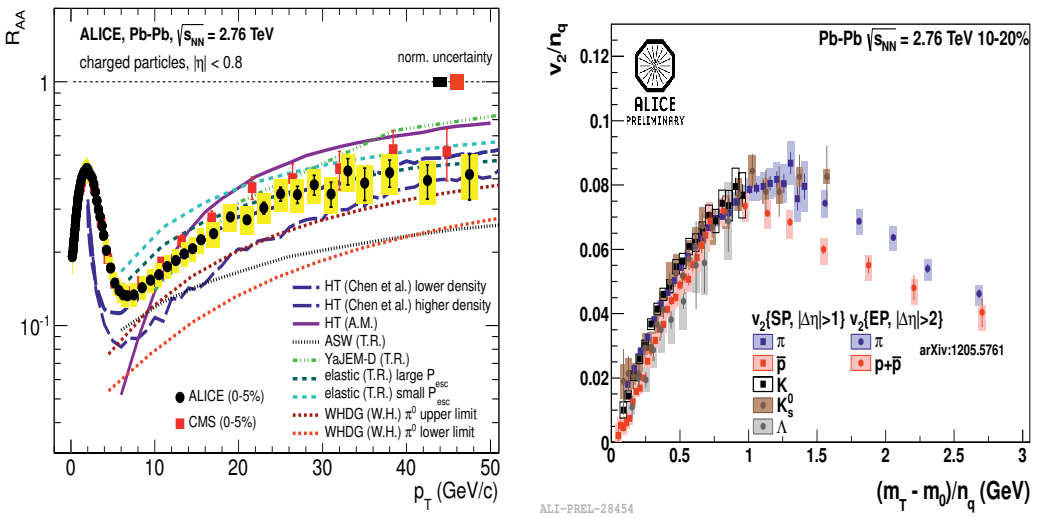

Figure 3. (Left) The nuclear modification factor R_{AA} measured at the LHC for the 5% most central Pb–Pb collisions, compared to model calculations. (Right) The charged particle pseudo–rapidity density dependence of R_{AA} in different p_{T}–intervals.

Here the number of binary nucleon–nucleon collisions $\langle N_{coll} \rangle$, is given by the product of the nuclear overlap function T_{AA} calculated from the Glauber model [22], and the inelastic NN cross–section $\sigma^{NN}_{inel.}$.

Parton energy loss was first observed at RHIC [3], where it was reported that the particle production in the 5% most central Au–Au collisions at $\sqrt{s_{NN}}$ = 200 GeV is suppressed by a factor of 5 at p_{T} = 5–6 GeV/c and is independent of p_{T} up to a value of 20 GeV/c. Figure 3–left presents the nuclear modification factor measured in the 5% most central Pb–Pb collisions at $\sqrt{s_{NN}}$ = 2.76 TeV [23]. The ALICE points, represented by the full circles are compared to the CMS result [24] (full squares). Both measurements agree within the uncertainties. It is seen that the data points exhibit a pronounced maximum at low p_{T} ($p_{\mathrm{T}} \approx$ 2 GeV/c) which could be another manifestation of collective radial flow [25]. At higher values of p_{T}, R_{AA} has a minimum at p_{T} = 5–7 GeV/c with a value of $R_{AA} \approx 0.13$. The minimum that is reached at the LHC is slightly lower than the relevant value at RHIC, where $R_{AA} \approx 0.2$. Beyond 7 GeV/c, the nuclear modification factor increases, reaching a value of ≈ 0.4 for $p_{\mathrm{T}}>$ 30 GeV/c. In the same figure, the experimental points are compared to model calculations that used RHIC data to calibrate the medium density and a variety of energy loss mechanisms [26]. Many of the curves can produce qualitatively the increase of R_{AA} with increasing p_{T}.

Figure 3–right presents the dependence of R_{AA} on the charged particle pseudo–rapidity density ($dN_{ch}/d\eta$). The markers correspond to different p_{T}–intervals. The strongest $dN_{ch}/d\eta$ dependence is reported for the interval $5 < p_{\mathrm{T}} < 7$ GeV/c. This dependence is gradually weakened at higher values of p_{T}. The LHC points are compared to results from RHIC for the p_{T}–interval where the relevant points were showing the largest suppression. It is seen that the LHC points exhibit a larger suppression in central collisions as one would expect for a system that is denser and lives longer in the deconfined phase. The value of R_{AA} for the most central RHIC collisions is very close to the relevant LHC value at a similar $dN_{ch}/d\eta$ of $\approx$ 700.

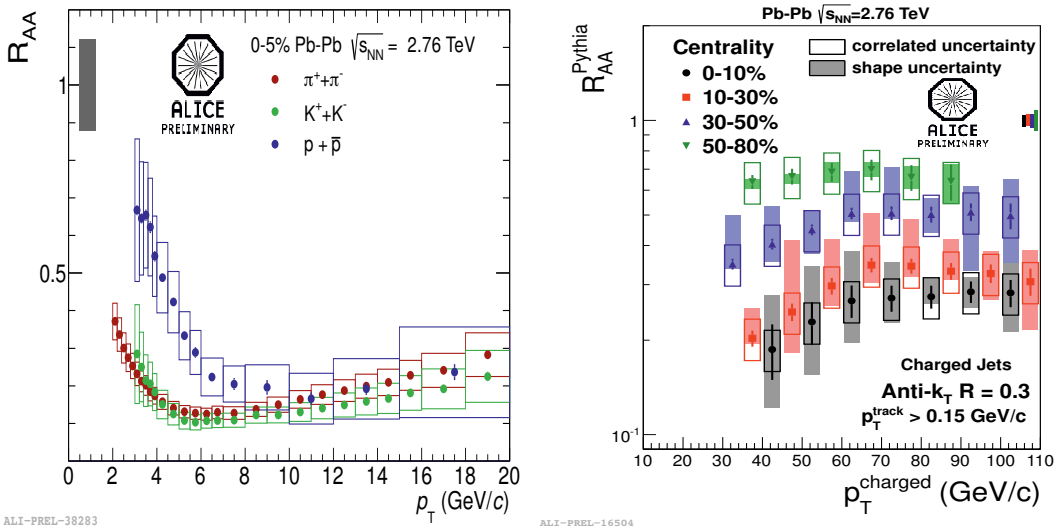

Figure 4. (Left) The nuclear modification factor R_{AA} for identified pions, kaons and protons measured at the LHC for the 5% most central Pb–Pb collisions [28]. (Right) The nuclear modification factor for jets measured with a radius of $R = 0.3$, where the the reference jet spectrum is extracted from PYTHIA Perugia0 [31].

Additional constrain on the models that attempt to describe the radiative energy loss could come by studying the production of identified particles. At the lower RHIC energies, it was found that the suppression depends on the type of particle i.e. mesons showed different suppression factors compared to baryons [27]. Figure 4–left presents the nuclear modification factor for pions, kaons and protons (i.e. positive and negative particles summed) for the 5% most central Pb–Pb collisions [28]. Particles were identified solely by the TPC, using the dE/dx information at the relativistic rise. It is seen that up to a p_{T} value of 6–7 GeV/c the meson curves overlap while the protons' R_{AA} is larger. The suppression seems to be the same for the different particle species for $p_{\mathrm{T}} > 10$ GeV/c, which could be interpreted as an indication that the fragmentation is not modified by the medium.

Studying the modification of fully reconstructed jets is also a useful tool for probing the properties of the deconfined system. Jets in ALICE are measured using charged particles reconstructed with the TPC and the ITS. For signal jets, the anti–k_{T} algorithm [29] was used while the background was measured with the k_{T} algorithm [30]. Figure 4–right shows the jet nuclear modification factor R_{AA}^{Pythia} for different centrality bins of Pb–Pb collisions [31]. A jet radius of $R = \sqrt{\Delta\varphi^2 + \Delta\eta^2} = 0.3$ was used, while the reference jet spectrum was extracted from Pythia. Similar to the single particle R_{AA}, the jets exhibit a strong suppression for central events, with R_{AA}^{Pythia} gradually increasing for more peripheral collisions.

4 Heavy flavor

The increased collision energy at the LHC compared to the previous highest energy at RHIC (almost a factor of 14), opens up the possibility to study high particle mass scales due to the much larger production cross–section of particles containing c and b quarks. It is believed that these heavy quarks

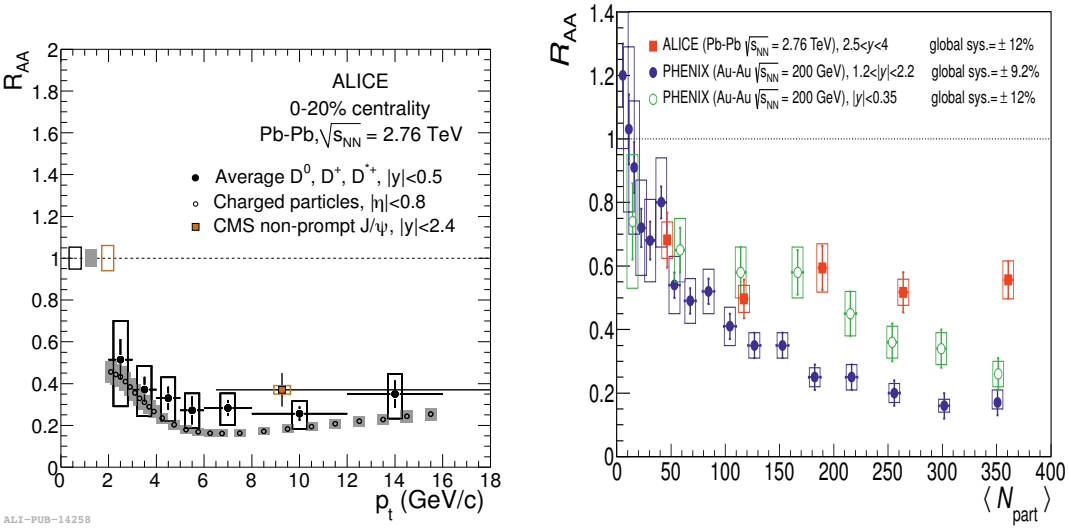

Figure 5. (Left). The nuclear modification factor for the average D–meson R_{AA} for the 20% central Pb–Pb collisions compared to charged particles and non–prompt J/Ψ from CMS [35]. (Right) The centrality dependence of the nuclear modification factor for inclusive J/Ψ, measured at forward rapidity ($2.5 < y < 4$) via the $\mu^+\mu^-$ channel with the muon spectrometer down to $p_{\rm T} = 0$ of the particle.

are produced at the initial stage of the creation of the system, with which they interact (parton energy loss), and are thought to probe its basic properties, such as the energy density. Based on QCD, the energy loss depends on the colour coupling factor, predicting that gluons should lose a larger amount of energy compared to quarks [32]. In addition, the in–medium effects are expected to be further reduced for heavy quarks due to a reduced small angle gluon radiation i.e. the "dead–cone effect" [33].

Figure 5–left presents the nuclear modification factor for the 20% most central Pb–Pb collisions, calculated as the average of the relevant factors for D^0, D^+ and D^{*+} mesons [34]. The D–meson signals were extracted using displaced decay vertex reconstruction of the hadronic decay channels: $D^0 \rightarrow K^-\pi^+$, $D^+ \rightarrow K^-\pi^+\pi^+$, and $D^{*+} \rightarrow D^0\pi^+$. The raw yields were feed–down corrected for contributions from B–decays using perturbative QCD predictions and Monte Carlo simulations. It is seen that the D–mesons are suppressed by a factor of 3–4, reaching a minimum of $R_{AA} \approx 0.25$ at $p_{\rm T}$= 5–6 GeV/c. The results are compared to the R_{AA} of charged particles and are found to be very close to each other. However, from this comparison there is an indication that $R_{AA}^{D} > R_{AA}^{charged}$. The same plot shows the results from the CMS Collaboration [35] for non–prompt J/Ψ mesons with $p_{\rm T}$> 6.5 GeV/c, where the suppression is weaker. The resolution of whether we observe the "dead–cone effect" will have to wait until we acquire more statistics.

Figure 5–right shows the nuclear modification factor for inclusive J/Ψ measured by ALICE as a function of the mean number of participating nucleons [36]. The J/Ψ is measured at forward rapidity ($2.5 < y < 4$) via the $\mu^+\mu^-$ channel with the muon spectrometer down to $p_{\rm T} = 0$. The ALICE points represented by the full squares show little centrality dependence and exhibit a centrality integrated $R_{AA}^{0\%-80\%} = 0.545 \pm 0.032$ (stat.) ± 0.083 (syst.). Compared to RHIC measurements at forward rapidity

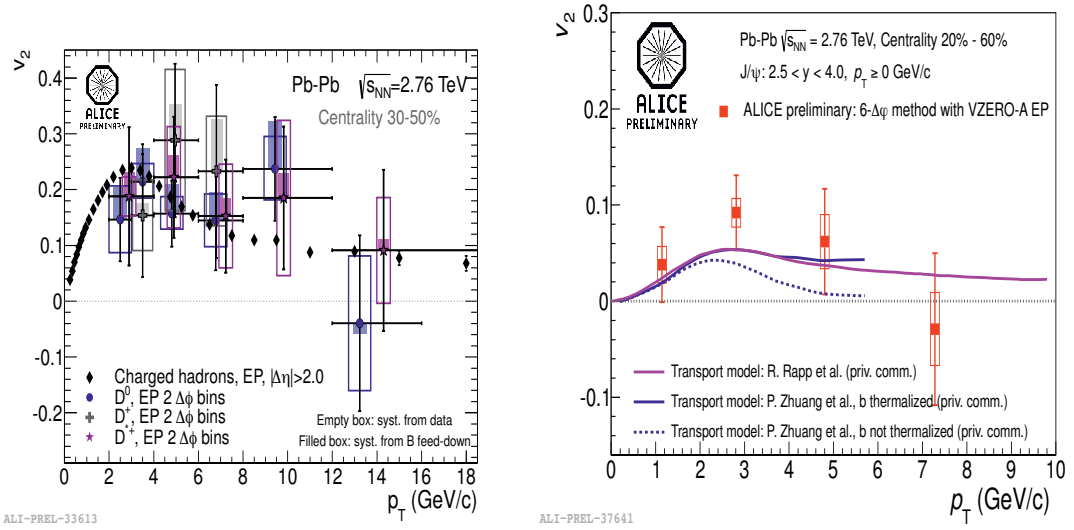

Figure 6. The p_T–differential v_2 measurements of D–mesons measured at mid–rapidity (left) and inclusive J/Ψ measured at forward rapidity (tight).

[37], we see that the LHC reported R_{AA} is twice as large in central collisions. Although the results are qualitatively in agreement with the expectation of a recombination scenario, where regeneration effects could be important at low values of transverse momentum, there are still quite a few things that need to be clarified and checked thoroughly before any firm conclusion could be drawn.

One other key question that could be addressed at the LHC, is whether the low–momentum heavy quarks could thermalize in the dense environment where they are created. A way to probe the degree of thermalisation is to look at the elliptic flow of c and b quarks. A step towards this direction was made by measuring the p_T–differential v_2 for prompt D–mesons, as shown in Fig. 6–left for the 30–50% centrality range. The results show a finite v_2 value with a significance of 3σ in the p_T range $2 < p_T < 6$ GeV/c. A similar study was performed for the J/Ψ measured at forward rapidities. The results are shown in Fig. 6–right for the 20–60% centrality range. A non–zero value of v_2 is also reported in this case for a similar range of p_T.

5 Parity violation studies

Parity (P) and its combination with the charge conjugation (C) symmetries is known to be broken in the weak interaction. However, in the strong interaction the P and CP invariances are respected, making the strong CP problem [38] one of the remaining puzzles of the Standard Model. The possibility to observe parity violation in the hot and dense hadronic matter, using relativistic heavy–ion collisions has been discussed for many years. According to various theoretical approaches, in the vicinity of the deconfinement phase transition, the QCD vacuum could create domains, local in space and time, that could lead to CP violating effects [39]. These effects could manifest themselves via a charge separation along the direction of the system's angular momentum or, equivalently, along the direction of the strong $\approx 10^{18}$ G, magnetic field created in non-central heavy–ion collisions and perpendicular to the reaction plane (the plane of symmetry of a collision defined by the impact parameter vector and the

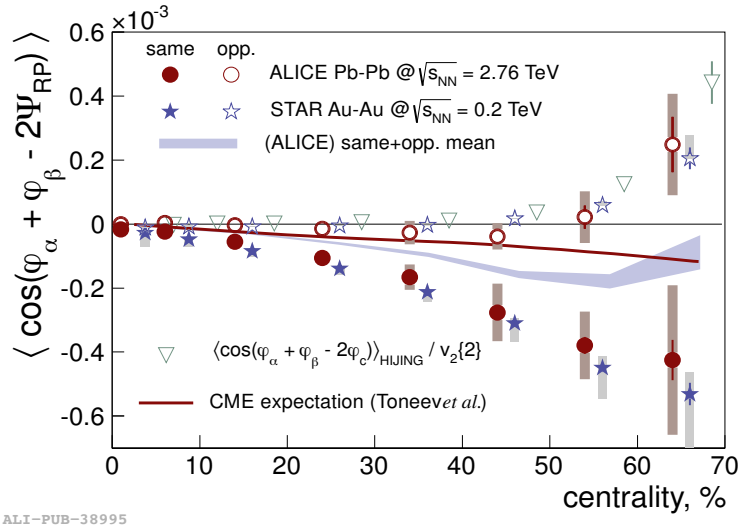

Figure 7. The centrality dependence of the $\langle\cos(\varphi_\alpha + \varphi_\beta - 2\Psi_{RP})\rangle$. The LHC results [41], represented by the full and open circles for the pairs of particles with same and opposite charge, respectively, are compared to results from RHIC [42] and to expectations from theory calculation [43] (see text for more details).

beam direction). This phenomenon is called the Chiral Magnetic Effect (CME). Due to fluctuations in the sign of the topological charge [40] of these domains, the resulting charge separation averaged over many events is zero. This makes the observation of the CME possible only via *P*–even observables, expressed in terms of two– and multi–particle correlations.

The ALICE Collaboration has studied the charge–dependent azimuthal particle correlations at mid–rapidity in Pb–Pb collisions at the centre of mass energy per nucleon pair $\sqrt{s_{NN}}$ = 2.76 TeV [41]. A multi–particle correlator was employed which probes the magnitude of the potential signal while at the same time suppresses the background correlations unrelated to the reaction plane. This correlator has the form $\langle\cos(\varphi_\alpha + \varphi_\beta - 2\Psi_{RP})\rangle$, where φ is the azimuthal angle of particles while the index indicates the charge or the particle type. The orientation of the reaction plane angle is represented by the Ψ_{RP}, and is estimated by constructing the event plane using azimuthal particle distributions.

Figure 7 presents the correlator $\langle\cos(\varphi_\alpha + \varphi_\beta - 2\Psi_{RP})\rangle$ as a function of the collision centrality compared to results from RHIC energies [42] and to model calculations [43]. The ALICE points, shown as full and open red markers for the pairs with same and opposite charge, respectively, indicate a significant difference in the magnitude but also in the sign of the correlations for different charge combinations, consistent with the qualitative expectations for the Chiral Magnetic Effect. The effect gets more pronounced as we move from central to peripheral collisions i.e. moving from left to right along the x–axis. The previous measurement of charge separation by the STAR Collaboration in Au–Au collisions at $\sqrt{s_{NN}}$ = 0.2 TeV [42], also shown in Fig. 7 (blue stars), is in qualitative but also quantitative agreement with the LHC measurement.

The thick solid line in Fig. 7 shows a prediction for the same sign correlations due to the Chiral Magnetic Effect at the LHC energies, based on a model that make certain assumptions about the

duration and time evolution of the magnetic field [43]. This model underestimates the observed magnitude of the same sign correlations seen at the LHC. However, calculations based on assumptions related to the initial time that the magnetic field develops as well as the same value of the magnetic flux for both energies, suggested that the Chiral Magnetic Effect might have the same magnitude at both collider energies [44]. Conventional event generators such as HIJING, that do not include any P–violating effects, do not exhibit any significant difference between the correlations of pairs with same and opposite charge (green triangles) and were averaged in the figure.

An alternative explanation to the Chiral Magnetic Effect assumption was recently provided by a hydrodynamical calculation [45], suggesting that the correlator under study may have a negative (i.e. out–of–plane), charge independent, dipole flow contribution originating from fluctuations in the initial condition of a heavy–ion collision. This could lead to a shift of the baseline, which coupled to another well known effect that is currently considered, the one of local charge conservation induced in a medium exhibiting strong azimuthal (i.e. elliptic) modulations, could in principle give a quantitative description of the centrality dependence observed from both collaborations [46]. Our results for the charge independent correlations are presented by the blue band in Fig. 7.

The measurements are supplemented by a differential analysis and will be extended with a study on higher harmonics but also investigating the correlations of identifying particles. These studies are expected to distinguish and quantify the different background sources.

6 Summary

With the LHC completing its third year of operation, the field of heavy–ion physics enters a new phase where precision measurements along with the quantification of the basic properties of the system that is formed in interactions of heavy ions become the main focus. The ALICE detector, designed and built for the study of heavy–ion collisions at the LHC, performed very well. The rich production of new physics results in this new energy regime revealed already significant information about the nature of the system created in Pb–Pb collisions at $\sqrt{s_{NN}} = 2.76$ TeV.

The further analysis of the already recorded data sample, but also the upcoming p–Pb data taking period at the beginning of 2013 will provide additional constrains to improve our understanding of the properties of the quark–gluon plasma.

References

[1] S. Borsanyi, JHEP **1011**, (2010) 077.

[2] H. Satz, Rep. Prog. Phys. **63**, (2000) 1511;
S.A. Bass, M. Gyulassy, H. Stöcker, W. Greiner, J. Phys. **G25**, (1999) R1;
E.V. Shuryak, Phys. Rep. **115**, (1984) 151;
J. Cleymans, R.V. Gavai, E. Suhonen, Phys. Rep. **130**, (1986) 217.

[3] I. Arsene *et al.* [BRAHMS Collaboration], Nucl. Phys. **A757**, (2005) 1.
K. Adcox *et al.* [PHENIX Collaboration], Nucl. Phys. **A757**, (2005) 184.
B. B. Back *et al.* [PHOBOS Collaboration], Nucl. Phys. **A757**, (2005) 28.
J. Adams *et al.* [STAR Collaboration], Nucl. Phys. **A757**, (2005) 102.

[4] K. Aamodt *et al.* [ALICE Collaboration], Phys. Rev. Lett. **105**, (2010) 252302.
K. Aamodt *et al.* [ALICE Collaboration], Phys. Rev. Lett. **107**, (2011) 032301.

[5] G. Aad *et al.* [ATLAS Collaboration], Phys. Rev. Lett. **105**, (2010) 252303.
K. Aamodt *et al.* [ALICE Collaboration], Phys. Lett. **B696**, (2011) 30.

[6] K. Aamodt *et al.* [ALICE Collaboration], J. Phys. **G30**, (2004) 1517;
K. Aamodt *et al.* [ALICE Collaboration], J. Phys. **G32**, (2006) 1295.
[7] K. Aamodt *et al.* [ALICE Collaboration], JINST **3**, (2008) S08002.
[8] K. Aamodt *et al.* [ALICE Collaboration], Phys. Rev. Lett. **105**, (2010) 252301.
[9] S. S. Adler *et al.* [PHENIX Collaboration], Phys. Rev. **C71**, (2005) 034908.
[10] J. Bjorken, Phys. Rev. **D27**, (1983) 140.
[11] K. Krajczar (for the CMS Collaboration), J. Phys. **G38**, (2011) 124041.
[12] P. Kolb and U. Heinz, arXiv:nucl-th/0305084
[13] B. Abelev *et al.* [ALICE Collaboration], arXiv:1208.1974 [hep-ex].
[14] B. Abelev *et al.* [STAR Collaboration], Phys. Rev. **C79**, (2009) 034909.
[15] S. S. Adler *et al.* [PHENIX Collaboration, Phys. Rev. **C69**, (2004) 034909.
[16] C. Shen *et al.*, Phys.Rev. **C84**, (2011) 044903.
[17] Y. Karpenko and Y. Sinyukov, J.Phys. **G38**, (2011)124059.
Y. Karpenko, Y. Sinyukov, and K. Werner, nucl-th/1204.5351.
[18] P. Bozek, Phys. Rev. **C85**, (2012) 034901.
[19] E. Schnedermann, J. Sollfrank, and U. W. Heinz, Phys. Rev. **C48**, (1993) 2462.
[20] S. Voloshin and Y. Zhang, Z. Phys. **C70**, (1996) 665.
A. M. Poskanzer and S. Voloshin, Phys. Rev. **C58**, (1998) 1671.
[21] B. Abelev *et al.* [STAR Collaboration], Phys. Rev. Lett. **99**, (2007) 112301.
[22] M. Muller *et al.*, Annu. Rev. Nucl. Part. Sci. **57**, (2007) 205.
[23] B. Abelev *et al.* [ALICE Collaboration], arXiv:1208.2711 [hep-ex].
[24] S. Chatrchyan *et al.* [CMS Collaboration], Eur. Phys. J. **C72**, (2012) 1945.
[25] B. Muller, J. Schukraft and B. Wyslouch, arXiv:1202.3233 [hep-ex].
[26] W. A. Horowitz and M. Gyulassy, Nucl. Phys. **A872**, (2011) 265.
C. A. Salgado and U. A. Wiedemann, Phys. Rev. **D68**, (2003) 014008.
X. F. Chen *et al.*, Phys. Rev. **C84**, (2011) 034902.
A. Majumder and B. Muller, Phys. Rev. Lett. **105**, (2010) 252002.
T. Renk *et al.*, Phys. Rev. **C84**, (2011) 014906.
T. Renk, Phys. Rev. **C83**, (2011) 024908.
[27] B. Abelev *et al.* [STAR Collaboration], Phys. Rev. Lett. **97**, (2006) 152301.
[28] P. Christiansen (for the ALICE Collaboration), arXiv:1208.5368 [nucl-ex].
[29] M. Cacciari, G. P. Salam and G. Soyez, JHEP **0804**, (2008) 063.
[30] M. Cacciari, G. P. Salam, Phys. Lett. **B641**, (2006) 57.
[31] M. Verweij (for the ALICE Collaboration), Nucl. Phys. **A**, (2012) 1.
[32] A. Majumder, M. van Leeuwen, Prog. Part. Nucl. Phys. **A66**, (2011) 41.
[33] Y. L. Dokshitzer, D. Kharzeev, Phys. Lett. **B519**, (2001) 199.
[34] B. Abelev *et al.* [ALICE Collaboration], arXiv:1203.2160 [nucl-ex].
[35] S. Chatrchyan (for the CMS Collaboration), JHEP **1205** (2012) 063.
[36] B. Abelev *et al.* [ALICE Collaboration], Phys.Rev.Lett. **109**, (2012) 072301.
[37] A. Adare *et al.* [PHENIX Collaboration], Phys. Rev. Lett., **98**, (2007) 232301.
A. Adare *et al.* [PHENIX Collaboration], Phys. Rev., **C84**, (2011) 054912.
[38] V. Baluni, Phys. Rev. **D19**, 2227 (1979).
R. J. Crewther *et al.*, Phys. Lett. **B88**, 123 (1979).
[39] D. Kharzeev, R. D. Pisarski and M. H. G. Tytgat, Phys. Rev. Lett. **81**, 512 (1998).

D. Kharzeev and R. D. Pisarski, Phys. Rev. **D61**, 111901 (2000).
[40] S. S. Chern, J. Simons, Ann. Math. **99**, 48 (1974).
[41] B. Abelev *et al.* [ALICE Collaboration], arXiv:1207.0900 [nucl-ex].
[42] B. I. Abelev *et al.* [STAR Collaboration], Phys. Rev. Lett. **103**, 251601 (2009).
B. I. Abelev *et al.* [STAR Collaboration], Phys. Rev. **C81**, 54908 (2010).
[43] V. D. Toneev and V. Voronyuk, arXiv:1012.1508 [nucl-th].
[44] D. Kharzeev, L. D. McLerran and H. J. Warringa, Nucl. Phys. **A803**, 227 (2008).
A. R. Zhitnitsky, Nucl. Phys. **A853**, 135 (2011).
[45] D. Teaney and L. Yan, Phys. Rev. **C83**, 064904 (2011).
[46] S. Schlichting and S. Pratt, Phys. Rev. **C83**, 014913 (2011).
S. Pratt, S. Schlichting and S. Gavin, Phys. Rev. **C84**, 024909 (2011).